

Stress softening of multigraft copolymers

R. Schlegel^a, D. Wilkin^a, Y. Duan^{a,1}, R. Weidisch^{a,*}, G. Heinrich^b, D. Uhrig^c, J.W. Mays^{c,d}, H. Iatrou^e, N. Hadjichristidis^e

^aInstitute of Materials Science and Technology (IMT), Friedrich-Schiller-University, Jena Lobdergraben 32, D-07743 Jena, Germany

^bLeibniz Institute of Polymer Research Dresden e.V., Hohe Strae 6, D-01069 Dresden, Germany

^cCenter for Nanophase Materials Sciences, Oak Ridge National Laboratory, Oak Ridge, TN 37831, USA

^dDepartment of Chemistry, University of Tennessee, Knoxville, TN 37996, USA

^eDepartment of Chemistry, University of Athens, Athens 157 71, Greece

ARTICLE INFO

Article history:

Received 2 June 2009

Received in revised form

28 September 2009

Accepted 12 October 2009

Available online 11 November 2009

Keywords:

Stress softening

Multigraft copolymers

Molecular architecture

ABSTRACT

The hysteresis behaviour of multigraft (MG) copolymers, with a polyisoprene backbone and polystyrene (PS) side chains, was investigated by applying a modified softening model proposed by Elas-Zuniga, which uses an approach of Ogden and Roxburgh. The model was combined with the non-affine tube model of rubber elasticity of Kaliske and Heinrich. Four parameters are obtained: chemical and physical cross-link moduli (G_c , G_e), the number of statistical segments between two successive entanglements (n_e/T_e) and a softening parameter (b). The model was proven to be valid by a comparison with other methods evaluating hysteresis behaviour. The characterization of the multigraft copolymers revealed a branch point and molecular architecture dependence of the softening parameter. b was low for tetrafunctional MG copolymers with cylindrical microdomains, and it was further reduced for a spherical morphology and for more complex molecular architectures. The magnitude of b also depends on the PS arm molecular weight for hexa- and tetrafunctional multigraft copolymers.

© 2009 Elsevier Ltd. All rights reserved.

1. Introduction

Multigraft copolymers are thermoplastic elastomers showing appropriate high tensile stress and high strains at break, up to about 1550% [1]. The tensile properties can be controlled by both molecular architecture and morphology, which makes it sometimes difficult to distinguish the influence of each clearly. The polymer chains of the investigated materials consist of a rubbery polyisoprene (PI) backbone with grafted polystyrene (PS) branches. The functionality of the branch points (tri-, tetra- or hexafunctional) is controlled by synthesis. The materials show microphase separated morphologies, which depend not only on the PS content and functionality but also on the number of branch points [2]. Because of high strains at break and low residual strains in hysteresis tests the term superelasticity was chosen to describe the behaviour of these materials [3]. Since strain independent quantification of elasticity at high strains is difficult due to the dependence of the residual strain ϵ_{res} on parameters like sample dimensions and maximum applied

strain, there is the need to characterize hysteresis more clearly. Several approaches are available in the literature describing the softening of elastomers [4–6], which results from the Mullins effect [7]. Models are divided into phenomenological, physical (microstructural rupture, microstructural changes, filled rubbers) and macromolecular based ones (models with an understandable physical source but not related quantitatively to measurable physical quantities). It is stated that even for physical models a correspondence to measurable physical values does not always exist, and often a large number of parameters are obtained, which are difficult to relate to materials properties [7]. To find a good compromise between applicability and significance, a modified energy-based softening model was chosen, combining a rubber elasticity model based on physical interpretations with an empirical softening function for the hysteresis unload curve.

2. Experimental

2.1. Materials

Synthesis of the multigraft copolymer and block-double-graft copolymers samples were described by Zhu et al. and Uhrig et al. [8,9]. Table 1 and Fig. 1 give an overview of the molecular characteristics of the investigated materials. Multigraft copolymers consist of

* Corresponding author. Fax: +49 3641947702.

E-mail address: roland.weidisch@uni-jena.de (R. Weidisch).

¹ Present address: Key Laboratory of Rubber-Plastics (QJST), Ministry of Education, Qingdao University of Science and Technology, Zhenzhou Road, Qingdao 266042, China

Table 1
Multigraft copolymer samples.

	PS content ϕ [vol.%]	Functionality n	Number of branch points β	Molecular weight M_w [kg/mol]
MG 4-15-5.3	15	Tetra	5.3	548
MG 4-15-8.5	15	Tetra	8.5	825
MG 4-23-3.2	23	Tetra	3.2	472
MG 4-23-6.6	23	Tetra	6.6	891
MG 6-21-2.7	21	Hexa	2.7	411
MG 6-21-5.2	21	Hexa	5.2	705
PS-PI(SI) ₄ -PS (BDG 1)	33	Tri	4	287

a PI-backbone chain with grafted PS arms as depicted in Fig. 1a and b. For multigraft copolymers a nomenclature was chosen, MG n - ϕ - β , where MG stands for regular multigraft, ϕ is the volume percent of PS and β refers to the average number of branch points per molecule in a given fraction. The block-double-graft copolymer consists of a PS-PI-PS triblock backbone and PI-PS diblocks, which are grafted, randomly spaced, on the rubbery middle block (Fig. 1c). The investigated reference material is a linear triblock copolymer (Kraton 1102) with 28 vol.% PS. The molecular architecture is illustrated in Fig. 1d.

1 wt.% solutions of block copolymer in toluene were prepared. The liquid was evaporated over 7 days, and the films were dried at 70 °C for 3 days under vacuum. Dog bone shaped specimens according ISO 527/type A (small sample size) were stamped from the films having a thickness of 0.1 mm.

2.2. Mechanical tests

The hysteresis tests were performed with a Zwick/Roell universal testing machine Z020 equipped with a 500N load cell

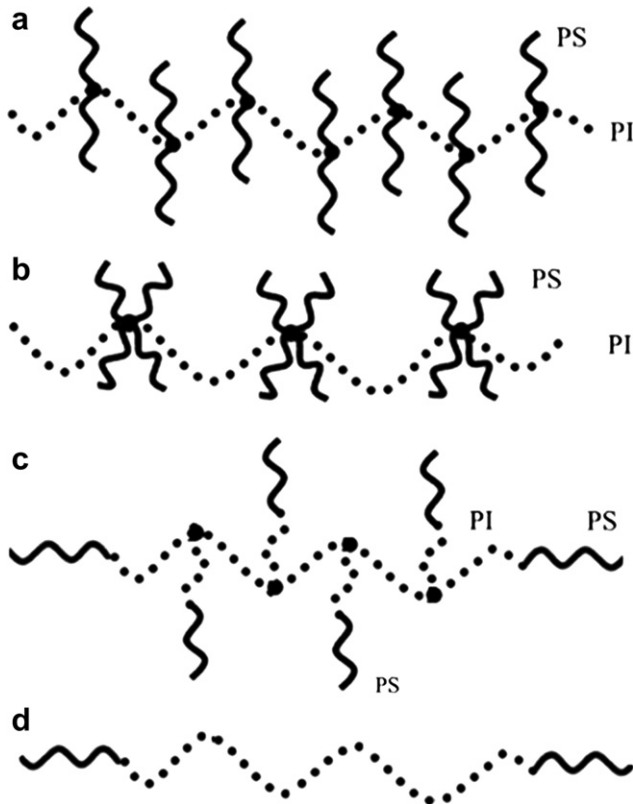


Fig. 1. Illustration of (a) tetrafunctional and (b) hexafunctional multigraft copolymers with regularly spaced junction points [2], (c) block-double-graft copolymer and (d) linear triblock copolymer.

(KAF-TC, A.S.T. GmbH Dresden, accuracy 0.05) at 23 °C, and the elongation was measured simultaneously by cross-head displacement ($l_0 = 10$ mm) and with an imaging system (Aramis, GOM). Hysteresis measurements were carried out at a cross-head speed of 15 mm/min. Although samples in tensile tests were tested at a lower strain rate ($l_0 = 45$ mm, 15 mm/min, 0.56%/s.), the same cross-head speed was chosen. The first cycle was performed up to 900% strain because this value was approximately the maximum strain for the reference material Kraton 1102. Most of the residual strain was observed to recover during the first few seconds after removing the samples from the clamps. After 5–10 min, which was approximately the time for image export and preparation for the new measurement, the second cycle was performed to 700%. By deforming the sample we expect an irreversible damage in the internal structure of the PS domains due to their glassy nature. The purpose of this procedure was to investigate the physical cross-linking imposed by the rubbery backbone between PS-PS domains of the fractured morphology without causing any further damage. Therefore, the maximum strain in the second cycle was set well below the previous deformation maximum. Additionally, the different values of the residual strain were taken into account in our analysis.

Each 5 s an image was taken from the stretched sample. The strain was calculated by measuring the distance between two marker positions when the measurement was finished. The load curve was fit to the non-affine tube model, while for the unload curve the softening model was applied using the parameters of the load curve as fixed values. The fits to the models were carried out by applying an interactive function and data plotting program (Gnuplot [10]).

2.3. Hysteresis softening model

The theory of the energy-based model of Elías-Zúñiga will be briefly reviewed [11]. The model is based on a pseudo-elastic model of Ogden and Roxburgh [12] to determine a softening function for the down cycle (Eq. 1).

$$\sigma = \eta(W, W_{\max})\sigma_0 \quad (1)$$

η is termed the continuous damage parameter, which satisfies the limits $0 < \eta \leq 1$. The strain-energy function of the Ogden and Roxburgh model is related to the pseudo-energy function \bar{W} given by Eq. 2.

$$\bar{W}(\lambda_1, \lambda_2, \eta) = \eta W(\lambda_1, \lambda_2) + \phi(\eta) \quad (2)$$

where $\phi(\eta)$ is a dissipation function, which was chosen in [11] by Eq. (3)

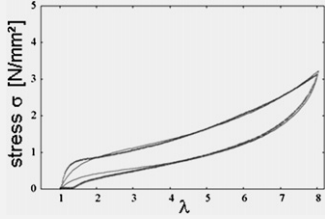
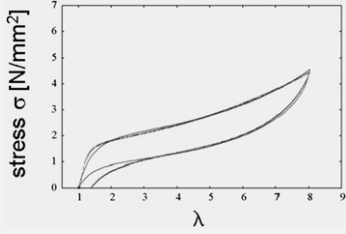
$$-\phi'(\eta) = -\left(\frac{1}{b}\ln(\eta)\right)^2 + W_{\max} \quad (3)$$

b is termed softening parameter. It was shown by Ogden and Roxburgh that the damage function satisfies the relation: $-\phi'(\eta) = W(\lambda_1, \lambda_2)$. A substitution in Eq. (3) yields the continuous damage parameter $\eta(W_{\max}, W(\lambda), b)$ in Eq. 4 with $W_{\max} = W(\lambda_{\max})$.

$$\eta = \exp\left(-b\sqrt{W_{\max} - W(\lambda)}\right) \quad (4)$$

Eq. 4 contains a strain energy function W and Eq. 1 the virgin material response σ_0 . The strain energy function was chosen from the extended tube model of Kaliske and Heinrich [13,14], where W consists of a cross-link and entanglement term: $W = W_c + W_e$ Eq. 5a. Considering uniaxial elongation ($\lambda_1 = \lambda$, $\lambda_2 = \lambda_3 = \lambda^{-1/2}$), and

Table 2
Comparison with other methods evaluating hysteresis behaviour.

parameter	Tetrafunctional	Kraton 1102
		
H_1	0.551	0.574
H_{1W}	0.607	0.607
b [(Nm) $^{-1/2}$]	0.221	0.171

deducing W with respect to λ , yields the stress response of the load curve given by Eq. 5b.

in load and unload curve (σ_{unload} , σ_{load}) and the ratio of hysteresis work of load and unload cycle (W_{unload} , W_{load}).

$$W = \frac{G_c}{2} \left(\frac{\left(\sum_{\mu=1}^3 \lambda_{\mu}^2 - 3 \right) \left(1 - \frac{T_e}{n_e} \right)}{1 - \frac{T_e}{n_e} \left(\sum_{\mu=1}^3 \lambda_{\mu}^2 - 3 \right)} + \ln \left(1 - \frac{T_e}{n_e} \left(\sum_{\mu=1}^3 \lambda_{\mu}^2 - 3 \right) \right) \right) + 2G_e \left(\sum_{\mu=1}^3 \lambda_{\mu}^{-1} - 3 \right) \quad (5a)$$

$$\sigma_0^{\text{load}} = G_c \left(\lambda - \frac{1}{\lambda^2} \right) \left(\frac{1 - \frac{T_e}{n_e}}{\left(1 - \frac{T_e}{n_e} \left(\lambda^2 + \frac{2}{\lambda} - 3 \right) \right)^2} - \frac{\frac{T_e}{n_e}}{1 - \frac{T_e}{n_e} \left(\lambda^2 + \frac{2}{\lambda} - 3 \right)} \right) + 2G_e \left(\frac{1}{\sqrt{\lambda}} - \frac{1}{\lambda^2} \right) \quad (5b)$$

This model contains 3 free parameters: the chemical and physical cross-link moduli (G_c , G_e) and the ratio n_e/T_e where n_e represents the number of segments between two successive entanglements in the bulk uncrosslinked polymer. T_e is the Langley trapping factor, which gives the probability that after cross linking a temporary entanglement will be trapped as a permanent entanglement. Hence, the ratio n_e/T_e can be considered as the average number of segments between two successive trapped entanglements in the polymer network. The substitution of Eq. 5a in 4 and 4 and 5b in Eq. 1 gives the stress response for the hysteresis down cycle (Eq. 6).

$$\sigma^{\text{unload}} = \sigma_0^{\text{load}} \exp \left(-b \sqrt{W_{\text{max}} - W(\lambda)} \right) \quad (6)$$

The softening parameters derived from the model fits were compared with other parameters evaluating hysteresis behaviour (Eqs. 7,8): the ratio of hysteresis stress at half maximum elongation

$$H_1 = \frac{\sigma_{\text{unload}}}{\sigma_{\text{load}}} \quad (7)$$

$$H_{1W} = \frac{W_{\text{unload}}}{W_{\text{load}}} \quad (8)$$

The purpose of this exercise is to quantify the distinctions between load and unload cycles. Two different materials were chosen, a tetrafunctional multigraft copolymer and Kraton 1102. Table 2 gives an overview of the obtained parameters. For H_{1W} similar values can be found, which are not suitable in distinguishing the two materials. The H_1 parameter is slightly higher for Kraton 1102, showing that the dissipated hysteresis work is slightly lower for the linear triblock, but the difference is only about 4%. The softening parameter reveals a much clearer distinction between the two materials. The b values differ by about 30%. The second important point is to clarify if the model parameters are independent of the maximum hysteresis strain. Such investigations are necessary since only cross-head displacement can be controlled. The maximum true strain was observed to vary within different materials due to clamp slippage. Hysteresis tests were carried out at 500, 700 and 900% strain and the softening model was applied. The findings are summarized in Table 3. It becomes obvious that in measuring strain by cross-head displacement, the model parameters are not constant and their deviations between 700 and 900% are high. The optical method yields clearly lower deviations, and up to 700–900% strain only minor changes can be observed. For all performed hysteresis tests at 900% cross-head displacement an optical strain of $873 \pm 70\%$

Table 3
Trend of model parameters at 900 and 700% strain for the tetrafunctional multigraft copolymer.

parameter	Trend	Deviation	Deviation	Deviation
	500–900% cross-head displ.	500–900% cross head	500–900% true strain	700–900% true strain
G_c	Increasing	8%	0.4%	~0%
G_e	Decreasing	7%	3.3%	0.8%
n_e/T_e	Increasing	26%	15%	2.5%
b	Decreasing	21%	10.4%	0.7%

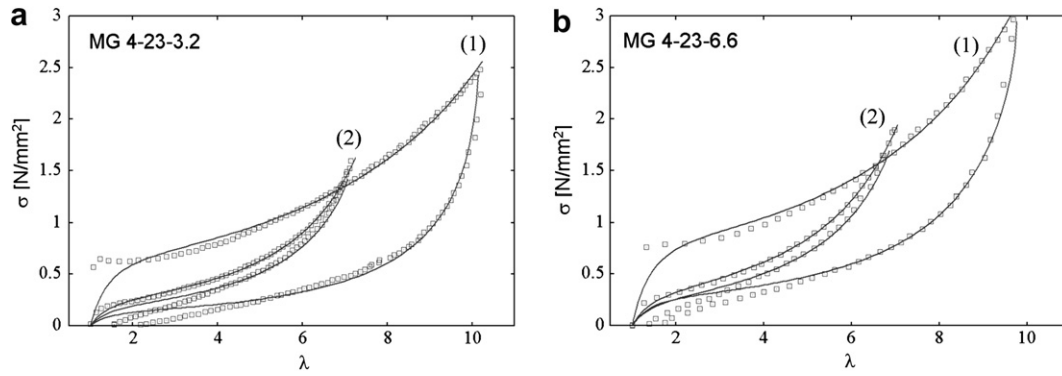


Fig. 2. Hysteresis curves of (a) MG 4-23-3.2 and (b) MG 4-23-6.6 at 900% and 700% strain.

and at 700% a maximum optical strain of $596 \pm 43\%$ was measured. As demonstrated in Table 3 the errors of the model parameters are minor up to 700–900% strain. This enables us to compare all obtained model parameters at 873% strain and all parameters obtained at 596% strain respectively, among each other. Therefore, we conclude that the model is suitable to identify small changes in hysteresis and that the parameters can be considered as independent from maximum hysteresis strain within a certain strain region.

3. Results and discussion

The discussion is structured in the following way: first the hysteresis of the multigraft copolymers at about 23–25 vol.% PS with different functionalities will be discussed, next we investigate the hysteresis behaviour of tetrafunctional multigraft copolymers

with about 15 vol.% PS forming spherical PS domains, and at the end of the discussion we will deal with the hysteresis and softening behaviour of the block-double-graft copolymer.

3.1. Tetrafunctional multigraft copolymer with 23 vol.% PS

In Fig. 2 a and b the hysteresis curves of the tetrafunctional multigraft copolymer with 23 vol.% PS at low and high number of branch points are shown. The model curves are fitting well to the experimental data, though yielding effects, as can be observed in the first deformation cycle, are not included in the model. Depicted are the hysteresis curves for initial deformation at 900% and at 700% strain. It can be observed from Fig. 2a and b that the final stress values are higher for MG 4-23-6.6 as compared to MG 4-23-3.2 in both cycles. The increase of the stress values appears also more pronounced in case of the multigraft with the higher number

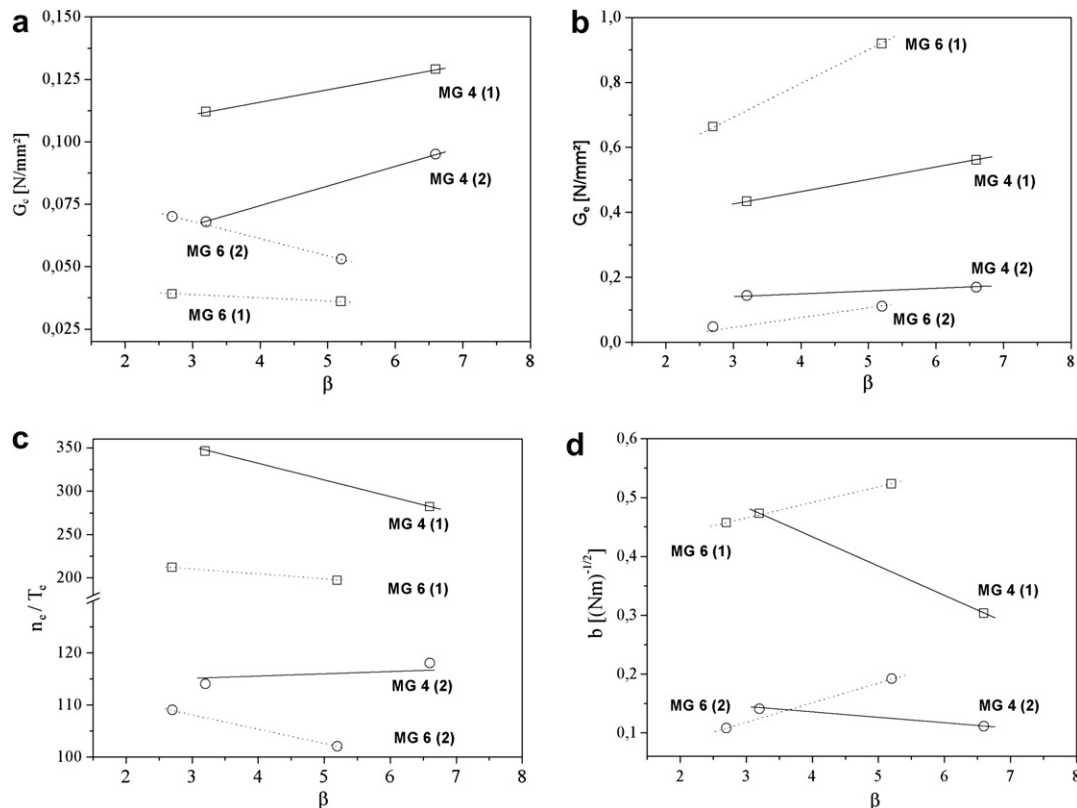


Fig. 3. Model parameters for MG 4-23- β and MG 6-21- β , (a) G_c , (b) G_e , (c) n_e/T_e and (d) b .

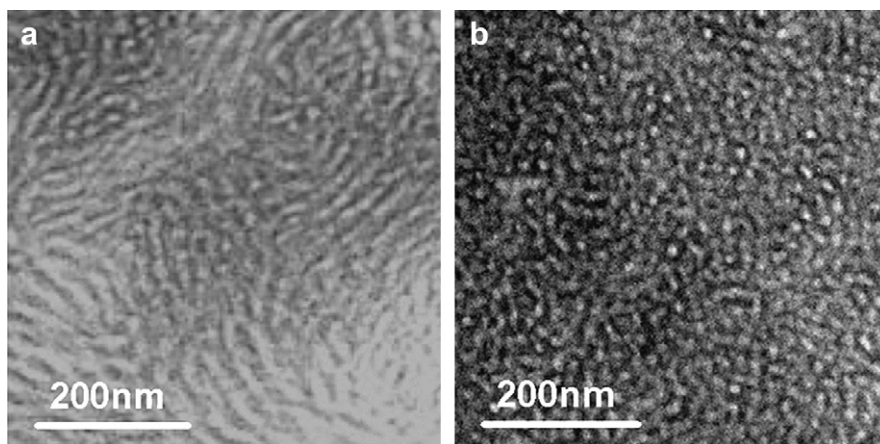


Fig. 4. Morphology of (a) MG 4-23-3.2 and (b) MG 4-23-6.6 [3,15].

of branch points. The obtained model parameters are plotted separately in Fig. 3a–d over the number of branch points. We will first discuss the parameters of the tetrafunctional multigraft copolymers.

While considering the data for the load curves at 900 and 700% strain, it can be observed that chemical and physical cross-link moduli are increasing with the number of branch points. An increase of G_c is logical since it is known that with an increase of β the morphology turns into a more disordered state and the number of PS domains are increasing [2]. Fig. 4 shows the morphology of the tetrafunctional multigraft with low (a) and higher (b) number of branch points. While the cylindrical PS domains in Fig. 3a are more continuous, the domains are well distributed in Fig. 3b. This effect corresponds to an increase in the number of chemical cross links. The G_c parameters for the second cycle are lower as compared to the first one, which is due to the damage of the initial morphology. Especially for a continuous PS phase it is difficult to correlate in the first cycle the chemical cross-link modulus with physical PS–PI–PS bridges. There the influence of morphology and molecular architecture interfere with each other.

A similar increasing trend can be found for the physical cross-link modulus G_e , which is related to the height of the plateau region. However, this parameter has to be considered carefully especially in case of very thin films. For such specimens, it is influenced remarkably by measuring errors of the sample dimensions. The decrease of n_e/T_e in Fig. 3c is consistent with the explanation given for G_c . The number of statistical segments are reducing if the cross-link density is increasing. The decrease of n_e/T_e in Fig. 3c

from first to second cycle reflects the pre-stretching of the molecular chains. It suggests irreversible intrinsic deformation of the elastomer backbone, which indicates to the formation of an increasing number of permanent entanglements. Finally, we can verify the increased cross linking with the number of branch points by the trend of the softening parameter b , which was obtained in the unload cycle. If the softening parameter is decreasing, the devolution of the unload curve is approaching the load curve. b is significantly decreasing with β . Between the first and the second cycle it is decreasing by about 63% for MG 4-23-6.6 and 70% for MG 4-23-3.2, indicating that there is less irreversible internal deformation in case of the better distributed and cross-linked PS phase.

It can be assumed that in the first cycle the casting morphology is breaking in the way that PS–PS bridges between different PS domains are fractured. Therefore the distribution of the PS and the amount of chemical cross links are increased by the deformation process. The G_c value obtained in the first cycle contains the influence of the unfractured morphology, and it is therefore not identical with the G_c of the second cycle.

3.2. Hexafunctional multigraft copolymer with 21 vol.% PS

Hysteresis curves at 900 and 700% with corresponding model fits for the hexafunctional multigraft copolymer are shown in Fig. 5a and b. The MG 6-23 material reveals a lamellae morphology at low number of branch points. In general a change in morphology from ordered to weakly ordered PS domains, as discussed for the tetrafunctional multigraft, was observed on going from low to high number of branch points. This was found by Zhu and co-workers [2]

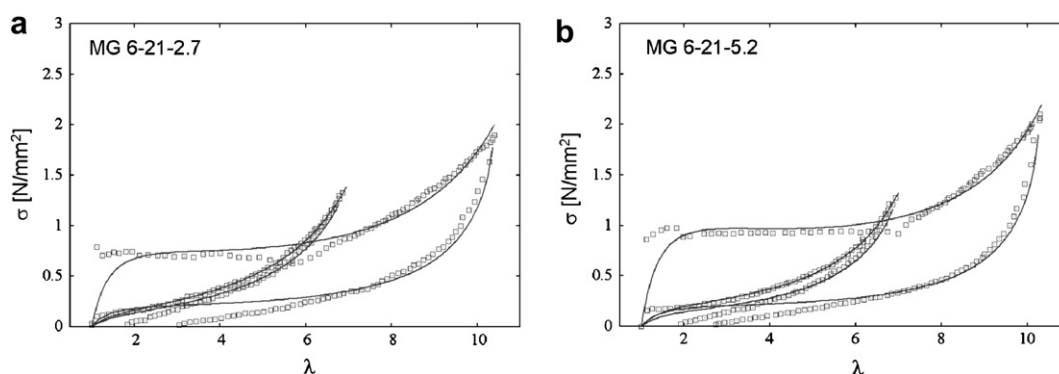


Fig. 5. Hysteresis curves of (a) MG 6-21-2.7 and (b) MG 6-21-5.2 at 900% and 700% strain.

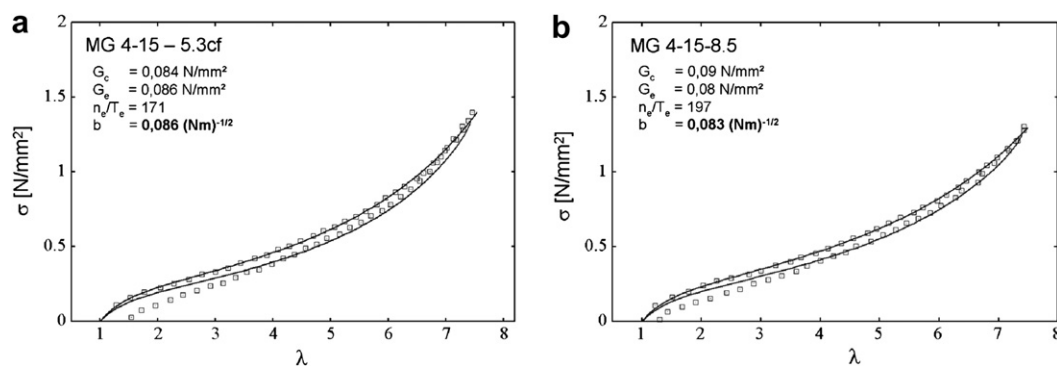


Fig. 6. Hysteresis curves of (a) MG 4-15-5.3 and (b) MG 4-15-8.5 at 700% strain (second cycle).

by SAXS and TEM investigations for the lamellae forming MG 6-type copolymers. Yielding becomes more important for the lamellar materials but also for cylindrical morphologies where the PS domains form an interconnecting network. However, this effect is discussed in recent work [16].

The increase of the hysteresis stress–strain curves in Fig. 5 is less pronounced as compared to the tetrafunctional multigraft. The materials show in the first cycle a pronounced plateau region with a sudden increase in the stress values. Further, it can be seen that the residual strain is higher as compared to the MG 4 – type, and in contrast the chemical cross-link modulus is decreasing with the number of branch points. Furthermore, it is significantly lower (Fig. 3a). Similar controversial observations can be made for the tendencies of b . The softening parameter is decreasing for tetrafunctional but increasing for hexafunctional multigraft copolymers with the increasing number of branch points (Fig. 3d). An explanation may be offered by considering the molecular architecture.

In thermoplastic elastomers (TPE) the mechanical strength is based on the physical cross linking between grafted PS arms [17]. The rubbery backbone is attached to the PS microdomains. In TPEs the PS domains act as multifunctional cross links. [18]. At room temperature the strength of these cross links is similar to that of chemically cross-linked rubbers. In case of low deformation, and if the PS phase forms an interconnecting structure, failure occurs due to breakage of cylinders or lamellae segments. If cylinders are well separated there is only orientation [19]. At high strains several other failure mechanisms become probable (molecular slippage, chain pull-out, chain disentanglement) [7]. It is clear for multigraft copolymers that, while keeping the PS content constant, by increasing the functionality from tetra- to hexafunctional the length of the PS arms are halved. Therefore, it can be assumed that the reduced PS arm length does not provide an effective coupling to the domains and that the short PS arms are pulled out of the domain. By increasing number of branch points the structure of the PS domains becomes more ramified, and this further reduces the connectivity of the PS arms. This suggests stronger PS–PS interaction in complex domains, and that the chain pull-out is more hindered in complex domains. The fact that at high number of branch points the tetrafunctional multigraft is showing lower

softening as compared to the hexafunctional material, but that at low β the opposite effect is observed, may additionally indicate that the chain pullout from larger lamellae is more hindered as compared to that from smaller ones. This is logical.

For G_c a decline with β at initial deformation was found in earlier works [16], and it was attributed to the initial break down of PS–PS domain bridges, which are easier to break for small PS–PS bridge type domains (disordered morphology). This was not always detected in the present investigations, suggesting that no perfect cylinders/lamellae are formed. In contrast to MG 6-21-5.2, the softening parameter is lower for MG 6-21-2.7 with a well ordered lamellar morphology. In general it must be stated that chain pull-out is the most probable failure mechanism for hexafunctional multigraft copolymers. The distance between the PS cross links is reduced, but as demonstrated by G_c and b its strength is weaker.

3.3. Tetrafunctional multigraft copolymer with 15 vol.% PS

The hysteresis data and model curves of the second cycle for tetrafunctional multigraft copolymer with 15 vol.% PS are shown in Fig. 6. The model parameters are inserted in the diagrams. The materials form spherical PS domains, and from literature data it can be concluded that the domain size is decreasing with the number of branch points [20]. Consequently, the number of PS domains (cross-link density) will increase. Considering the molecular architecture in contrast to the hexafunctional multigraft it can be found that even at the lower PS content the length of the PS arm is about 1.3 times higher. This results in a higher chemical cross-link modulus as compared to MG 6-21- β and even lowers the softening parameters. Further, the contribution of filler–filler rupture at small deformations is reduced for the spherical morphology as compared to cylindrical and lamellae. The b values are at about $0.08 \text{ (Nm)}^{-1/2}$ and are decreasing slightly with increasing number of branch points (Fig. 6). Due to the longer PS arms there is an improved PS–PS interaction in the domains, and additionally hydrodynamic pressure can be assumed to stabilize the spherical PS domains. This is making chain pull-out and rupture of the particles less probable. The increase of n_e/T_e with β indicates to higher strain at break values for MG 4-15-8.5. The observation is supported by the values from tensile tests for MG 4-15-5.3cf and MG 4-15-8.5, which are 1340% and 1432%, respectively. It can be assumed that in case of decreasing domain size the PS–PS interaction is also reduced. In Fig. 6 we can only observe a slight decrease of the softening parameter, and therefore it must be further assumed that improved physical cross linking because of several PS domains (decrease of b) and the reduced PS–PS interaction in smaller domains (increase of b) compensate each other.

Table 4
Model parameters for Kraton 1102 and BDG 1.

Parameter	Kraton 1102		BDG 1	
	800%	700%	900%	700%
G_c [N/mm ²]	0.37	0.12	0.45	0.3
G_e [N/mm ²]	1.11	0.94	0.93	0.45
n_e/T_e	132	65	222	75
b [(Nm) ^{-1/2}]	0.24	0.07	0.2	0.08

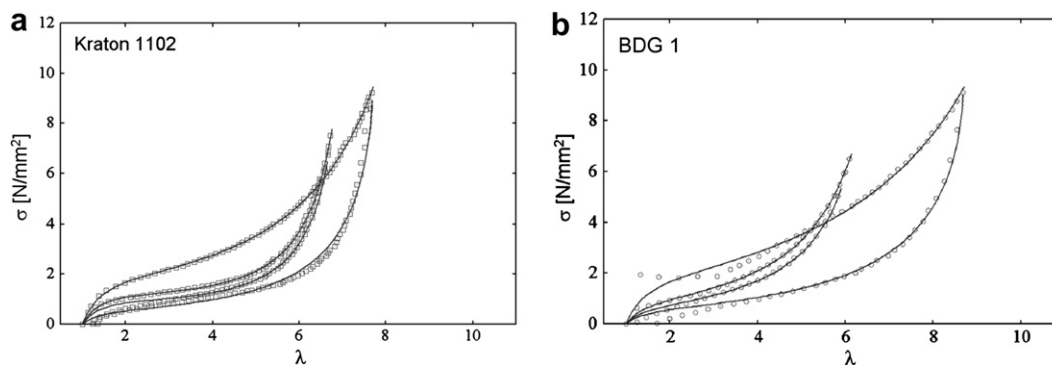


Fig. 7. Hysteresis curves of (a) Kraton 1102 and (b) BDG 1.

3.4. Complex molecular architecture, block-double-graft copolymers

In Fig. 7 the first and second hysteresis cycles of the block-double-graft copolymer BDG 1 and the commercial TPE Kraton 1102 are shown. The obtained model parameters are summarized in Table 4. Because of clamp slippage the first cycle for Kraton 1102 was performed at 800%. Both materials differ in their PS content slightly, which is about 28 vol.% for Kraton 1102 and about 33 vol.% for BDG 1. Synchrotron SAXS measurements for BDG 1 reveal a lamellae morphology with an interdomain distance of 29.5 nm. A distinct primary peak at $q = 0.214 \text{ nm}^{-1}$ and slight peaks at $2q^*$ and $3q^*$ indicating to this morphology type (Fig. 8). The morphology of Kraton 1102 is known from the literature, showing hexagonally packed PS cylinders with a domain distance of about 30 nm [19]. In pure SAXS measurements the peaks at $2q^*$ and $3q^*$ could not be observed, and an attempt was made to determine the interphase thickness for BDG 1 by applying the method of Ruland [21,22]. Less reasonable values of about 0.21 nm were found by this approach. Because of other peaks, which are impacting the slope in the region of interest, this was not possible to conduct for Kraton 1102.

The chemical cross-link modulus G_c for the complex architecture type is in both cycles clearly improved as compared to the linear triblock. Additional, its decrease from the first to second cycle is much lower.

Comparing the n_e/T_e values indicates to higher strain at break values for BDG 1, but experimental values show only slight differences (Kraton: $\varepsilon_B = 1050\%$, BDG 1: $\varepsilon_B = 1068\%$). The observed behaviour may be attributed to the molecular architecture of BDG 1

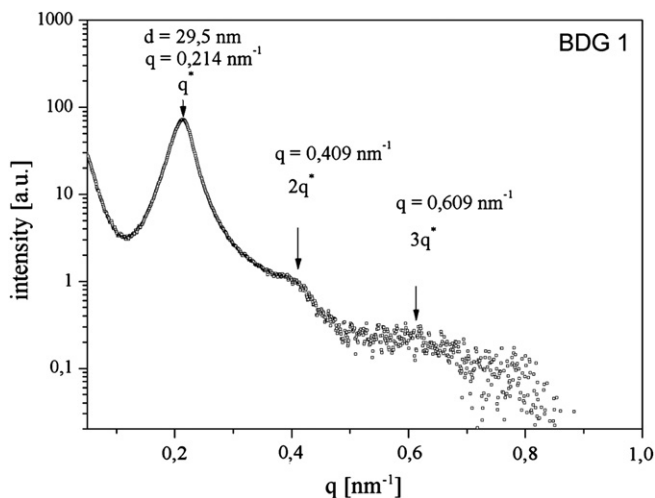


Fig. 8. Synchrotron SAXS pattern of BDG 1.

as compared to a triblock copolymer. The results show that the molecular architecture of BDG 1 is effective in providing high physical cross linking. The number of statistical segments is related to the up-turn region of the stress–strain curve. It is lower for the commercial material. The block-double-graft reveals a lower softening in the first and a comparable softening in the second cycle but it has to be noted that the PS content of BDG 1 is about 6 vol.% higher as compared to the commercial TPE. Nevertheless, lower and similar softening parameters are surprising. The parameters in Table 4 imply a high efficiency of the block-double-graft architecture and stronger ‘chemical’-PS cross links. The higher strength and elasticity of BDG 1 may be explained by the well cross-linked and dispersed PS domains with a soft interface and sufficient ratio of interface thickness to domain size, which prevents chain pull-out. Due to the occurrence of secondary and ternary peaks in the scattering pattern, it can be assumed that the discussed properties can be further improved by increasing the number of branch points.

4. Conclusion

The analysis of the hysteresis behaviour of multigraft copolymers has shown that important information can be deduced from the unload curve. This demonstrates also that changes in the morphology are reflected in the softening parameter, which is not elucidated by common methods evaluating hysteresis behaviour. In the experimental section, evidence was provided on nearly strain independent model parameters by measuring the true strain. The softening model was then applied to the hysteresis curves of multigraft copolymers, and the obtained model parameters were discussed in detail. Differences could be clearly shown between tetra- and hexafunctional multigraft copolymers at similar PS content. Since these two materials exhibit cylindrical and lamellar morphologies, respectively, the different properties cannot clearly attributed to the molecular architecture in the first hysteresis cycle. The second cycle at 700% strain provides more insight into the effects of molecular architecture. For tetrafunctional multigraft copolymers, at low PS content and spherical morphology, softening is lower as compared to the cylindrical morphology in the first and second cycles. These effects are attributed to hydrodynamic amplification of the PS spheres. Despite a lower PS content, the length of the PS arms is still longer in tetrafunctional multigrafts as compared to hexafunctional multigraft copolymers counteracting the chain pull-out. The softening behaviour characterisation method was also applied to a complex architecture of a block-double-graft copolymer consisting of a PS–PI–PS triblock and grafted diblocks. The analysis revealed that the softening characteristics of this TPE with 33 vol.% PS is similar to tetrafunctional MG copolymers at 23 vol.% PS during the first cycle, and in the second cycle it is comparable to the material with spherical PS domains. The softening behaviour was

found to be lower in the first cycle and similar in the second compared to the commercial TPE Kraton 1102. The chemical cross-link modulus was found to be higher in each cycle for the BDG 1 sample. Investigations of the morphologies are planned.

Acknowledgement

The authors thank for financial support of this work within the framework of the German Science Foundation (DFG). A portion of this research at Oak Ridge National Laboratory's Center for Nanophase Materials Sciences was sponsored by the Scientific User Facilities Division, Office of Basic Energy Sciences, U.S. Department of Energy (enabled through User Project # 2003–028) and supported in part by the Division of Materials Science and Engineering, Office of Basic Energy Sciences, U. S. Department of Energy (DE-AC05–00OR22725). The authors thank additionally Dr. Schneider at IPF Dresden for helpful discussions regarding the mechanical testing procedures and for performing the SAXS measurements at Deutsches Elektronen-Synchrotron (DESY) Hamburg.

References

- [1] Weidisch R, Gido SP, Uhrig D, Iatrou H, Mays JW, Hadjichristidis N. *Macromolecules* 2001;34:6333–7.
- [2] Zhu Y, Burgaz E, Gido SP, Staudinger U, Weidisch R, Uhrig D, et al. *Macromolecules* 2006;39:4428–36.
- [3] Duan Y, Thunga M, Schlegel R, Schneider K, Rettler E, Weidisch R, et al. *Macromolecules* 2009;42:4155–64.
- [4] Klüppel M, Meier J, Ramspeck M. III European Conference on Computational Mechanics Solids, Structures and Coupled Problems in Engineering, Lisbon 2006.
- [5] Dorfmann A, Ogden RW. *Int J Solid Struct* 2004;41:1855–78.
- [6] Kazakevičiūtė-Makovska R. *Int J Solid Struct* 2007;44:4145–57.
- [7] Diani J, Fayolle B, Gilormini P. *Eur Polym J* 2009;45:601–12.
- [8] Zhu Y, Weidisch R, Gido SP, Velis G, Hadjichristidis N. *Macromolecules* 2002;35:5903–9.
- [9] Uhrig D, Mays JW. *Macromolecules* 2002;35:7182–90.
- [10] Janert PK. *Gnuplot in action*. Manning Pubn; 2009.
- [11] Elías-Zúñiga A. *Polymer* 2005;46:3496–506.
- [12] Ogden RW, Dorfmann DG. *Proc R Soc London A* 1999;455:2861–77.
- [13] Kaliske M, Heinrich G. *Rubber Chem Tech* 1999;72:602–32.
- [14] Klüppel M, Schramm J. *Macromol Theory and Simul* 2000;9:742–54.
- [15] Staudinger U. Technische Universität Dresden, Dissertation; 2007.
- [16] Schlegel R, Staudinger U, Thunga M, Weidisch R, Heinrich G, Uhrig D, et al. *N Eur Polym J* 2009;45:2902–12.
- [17] Nielsen LE, Landel RF. *Mechanical properties of polymers and composites, chapter 5: stress–strain behaviour and strength*. CRC Press; 1994.
- [18] Holdon G, Legge NR. *Styrenic thermoplastic elastomers*. In: Holdon G, Legge NR, Quirk R, Schroeder HE, editors. *Thermoplastic elastomers*. Munich: Hanser; 1996. p. 54–8.
- [19] Morrison FA, Winter HH. *Macromolecules* 1989;22:3533–40.
- [20] Thunga M, Schlegel R, Staudinger U, Duan Y, Weidisch R, Heinrich G, et al. *KGK* 2008;09:597–605.
- [21] Zin WC, Roe RJ. *Macromolecules* 1984;17:183–8.
- [22] Ruland W. *Macromolecules* 1987;20:87–93.